Eur. Phys. J. D **40**, 247–255 (2006)
DOI: 10.1140/epjd/e2006-00150-y

THE EUROPEAN PHYSICAL JOURNAL D

A molecular dynamics description of clusters in strong laser fields

M. Belkacem[1], F. Megi[1], P.-G. Reinhard[2], E. Suraud[1], and G. Zwicknagel[2,a]

[1] Laboratoire de Physique Théorique, Université P. Sabatier, 118 route de Narbonne, 31062 Toulouse Cedex, France
[2] Institut für Theoretische Physik, Universität Erlangen, Staudtstrasse 7, 91058 Erlangen, Germany

Received 3 October 2005 / Received in final form 31 May 2006
Published online 28 June 2006 – © EDP Sciences, Società Italiana di Fisica, Springer-Verlag 2006

Abstract. We discuss from a theoretical perspective the energetic dynamics of clusters after irradiation with intense laser pulses in the regime of intensities larger than 10^{16} W/cm^2. To that end, we have developed a molecular dynamics (MD) model. The valence as well as the core electrons of each atom are treated as classical Coulomb interacting particles. A minimum of quantum information is embodied by associating a finite width to each electron which is adjusted to the energies and radii of the related atomic shells, thus being different for valence and core electrons. The model aims at high excitation but delivers satisfying physical properties for the initial phase of the process, i.e. it provides a stable cluster ground state and a reasonable description of optical response. We find that the pattern of electron emission versus laser intensity are well reproduced in comparison with fully quantum mechanical calculations. Finally, we produce first applications of the model to violent processes after strong laser irradiation for various medium large Na, Ar and Xe clusters.

PACS. 36.40.-c Atomic and molecular clusters – 02.70.Ns Molecular dynamics and particle methods

1 Introduction

Cluster dynamics is a very broad field of research covering so diverse phenomena as, e.g., thermodynamical properties, structure analysis using optical response, high impact collision, or the most violent laser excitations with subsequent Coulomb explosion, for an extensive discussion see [1]. Amongst all these processes, a subfield of its own with high current interest is the cluster fragmentation induced by high laser fields with intensities at and above $I = 10^{16}$ W/cm^2. This is the regime where the laser field suffices to ionize directly electrons from core states of the cluster atoms. The enormous forces at work lead to remarkable reaction products: high-energy electrons in the keV range [2], highly charged and very energetic ions [3], fragments [4], X-rays [5,6], and even neutrons from nuclear fusion reactions [7]. Most of these phenomena have been observed in a similar fashion for many different sorts of clusters, e.g, rare gases or metals and even up to organic material [8,9].

The theoretical description of these very energetic processes is a very demanding task and still in development. There exist already several different approaches, for recent reviews see [1,10]. All of them rely on (semi-)classical concepts because a quantum mechanical treatment becomes extremely expensive and is not really compulsory for these high excitation states. Most prominent are probably the models based on the concept of a nano-plasma and its various realizations [6,11–13]. A Thomas-Fermi approach is used in [14]. Dynamics according to the Vlasov equation is discussed, e.g., in [15]. A few more microscopic approaches are available, in particular molecular dynamics (MD) approaches [16–18] which provide in this context an interesting compromise between simplicity and microscopic detail. The calculations reported, e.g., in [18] used MD for valence electrons and rate equations to describe the tunneling of core electrons into the valence domain. In this paper, we carry on along the line of MD models. We aim at a conceptually simpler MD approach where core electrons and valence electrons are treated at the same level as classically Coulomb interacting particles. A minimum of quantum information is brought into the picture by associating a finite width to each electron. We will outline the model in detail, discuss proper calibration as well as various limiting cases, and provide finally a few first applications for medium large metal and raregas clusters.

2 The model

We describe a cluster as a set of electrons and ions of charge q_I, both treated as classical particles. Their dynamical degrees of freedom are position and momentum $(\mathbf{r}_i, \mathbf{p}_i)$. Each particle $i \in \{1...\mathcal{N}\}$ is represented by a Gaussian of fixed width σ_i. The interaction between particles (electrons and/or ions) is simply Coulombic. But because of the finite extension of the particles the Coulomb

[a] e-mail: zwicknagel@physik.uni-erlangen.de

interaction is here equivalent to a interparticle potential of the form

$$V_{ij}(r) = Q_{ij}\frac{\mathrm{erf}(r/\sigma_{ij})}{r} \tag{1}$$

with $\sigma_{ij}^2 = \sigma_i^2 + \sigma_j^2$ for particles i and j, $Q_{ij} = e^2$ for an electron-electron interaction, $Q_{ij} = -q_I e$ for an electron-ion interaction, $Q_{ij} = q_I^2$ for an ion-ion interaction, and $\mathrm{erf}(x) = 2\int_0^x \exp(-y^2)dy/\pi^{1/2}$.

In the initial state a (neutral) cluster is composed of N atoms each consisting of an ion of a charge $q_I = +n|e|$ and n electrons, that is, of $\mathcal{N} = (n+1)N$ particles in total. The width σ_i of the electrons is associated with that quantum state where they were sitting on initially. They are adjusted such that the energies of the electrons roughly match the quantal single particle energies, which, in turn, also tunes these finite widths to be of the order of the radius of that state. The finite width σ_I of the ions accounts for their net extension due to remaining deep core electrons bound to the actual ion. All ions have the same σ_I. Details and examples for the actual choice of the σ_i will be given in the next section. Fixing the widths in this way there are no free parameters in the model.

For the molecular dynamics (MD) calculations, we solve the classical Hamiltonian equations of motion

$$\begin{aligned}\frac{d\mathbf{r}_i}{dt} &= \frac{\mathbf{p}_i}{m_i}\\ \frac{d\mathbf{p}_i}{dt} &= -\sum_{j\neq i}\nabla_r V_{ij}(\mathbf{r}) + q_i\mathbf{E}_{\mathrm{laser}}(t)\end{aligned} \tag{2}$$

where the potential V_{ij} is given by equation (1), m_i, q_i are the mass and charge of particle i (electron or ion), respectively, and $\mathbf{E}_{\mathrm{laser}}(t)$ is the applied laser field. The equations of motion, equations (2), are solved using the velocity Verlet algorithm [19] and an adaptive timestep scheme. For the initial state of the cluster the positions of the ions are sampled stochastically in a sphere with a radius equal to the cluster radius R. During this sampling attention is paid to equilibrize the mutual distances between the ions by rejecting configurations with nearby ions. Finally the electrons are attached to the ions; details are given in the next section. In order to attain a statistically reasonable description we perform an ensemble of calculations starting with slightly different initial samples. Later on, each of these microscopic realizations will also be called an 'event'. Note finally that all initial momenta $\mathbf{p}_i(t=0)$ are set equal to zero.

3 Ground state properties

As test cases for the MD model we studied both sodium and rare gas clusters. Here we focus on three examples, Na_{41}^+, Ar_{80} and Xe_{80} clusters. The Na_{41}^+ cluster serves as a benchmark because we can compare directly with previously published calculations performed for moderate laser intensities by more microscopic approaches (quantal and semi-classical).

Table 1. Parameters for rare gas clusters and Na.

Element	Energies [eV]		Orbit radii [a_0]		Widths [a_0]		
	ϵ_v	ϵ_c	r_v	r_c	σ_I	σ_v	σ_c
Na	–5.1	–38.7	–	0.35	1	6.5	1
	ϵ_p	ϵ_s	r_p	r_s	σ_I	σ_p	σ_s
Ar	–15.8	–29.3	0.86	0.46	1.4	1.5	0.9
Xe	–12.5	–23.3	1.09	0.58	1.7	1.8	1.1

For the Na_{41}^+ cluster 9 electrons per atom, 8 "core" electrons with σ_c (sitting in the $2s$ and $2p$ shells) and one "valence" electron with σ_v (from the 3s shell) are considered, i.e. $\mathcal{N} = 40\times 9 + 8 + 41 = 409$ particles (41 ions, 40 $3s$ and 328 ($2s/2p$) electrons) per cluster. Because the $2s$ and $2p$ shells are energetically relatively close to each other we treat these two shells at the same footing by attributing its electrons the same width σ_c. For the rare gas clusters Ar_{80} and Xe_{80}, 8 electrons per atom are taken into account, 6 (valence) electrons with σ_p from the $3p$ shell for Ar and from the $5p$ shell for Xe and 2 (core) electrons with σ_s from the $3s$ and $5s$ shell, respectively. Thus $\mathcal{N} = 80\times 8 + 80 = 720$ particles are propagated here per cluster by the MD treatment.

The widths $\sigma_{c,s}$,$\sigma_{v,p}$ and σ_I of the core electrons, the valence electrons and the ion are calibrated with respect to the shell energies $\epsilon_{c,s}$ and $\epsilon_{v,p}$ of an isolated atom [20] and a final fine-tuning of the global properties of a whole cluster. For Na the core shell energy ϵ_c is taken as a weighted average over the $2s$ and $2p$ shells, while for Ar and Xe the ϵ_p is given by averaging over the $3p$ and $5p$ subshell energies, respectively. The actually used values are given in Table 1. The first step of the adjustment of the widths consists in fitting the shell energies. To that end, the design values $\epsilon_{c,s}, \epsilon_{v,p}$ are assumed to match the total potential energies $U_{c,s}$ and $U_{v,p}$ of a corresponding single electron, when all electrons of the atom are just sitting on top of the ion ($r_{Ie} = 0$). For a Na atom with 9 electrons (i.e. $Q_{Ie} = -9e^2$) we then arrive at

$$\begin{aligned}\epsilon_v = U_v &= V_{Iv}(0) + 8V_{cv}(0)\\ \epsilon_c = U_c &= V_{Ic}(0) + 7V_{cc}(0) + V_{cv}(0),\end{aligned} \tag{3}$$

where $V_{ij}(0) = Q_{ij}2/(\pi(\sigma_i^2+\sigma_j^2))^{1/2}$, $i,j = I,v,c$, is the interaction potential (Eq. (1)) evaluated at $r = 0$.

In the case of the rare gas atoms with 8 electrons ($Q_{Ie} = -8e^2$) the corresponding expressions are

$$\begin{aligned}\epsilon_p = U_p &= V_{Ip}(0) + 2V_{ps}(0) + 5V_{pp}(0)\\ \epsilon_s = U_s &= V_{Is}(0) + 6V_{sp}(0) + V_{ss}(0).\end{aligned} \tag{4}$$

The nonlinear equations (3) or (4) usually allow for infinitely many solutions. To proceed towards a definite and physical result we start the iteration procedure from some reasonable estimates for the 'core size' $\sigma_I/a_0 = 1, 1.4, 1.7$ for Na, Ar and xenon, respectively. From the multiple pairs (σ_v, σ_c) solving equations (3) or (4) next a physically reasonable (e.g. $\sigma_{v,p} \gtrsim \sigma_{c,s}; \sigma_{v,p}, \sigma_{c,s} \approx \sigma_I$) one is selected. For the discussed examples and the given $\epsilon_{v,p}, \epsilon_{c,s}$ we then arrive at $\sigma_c/a_0 = 1, \sigma_v/a_0 = 6$ for Na, $\sigma_s/a_0 = 0.83$,

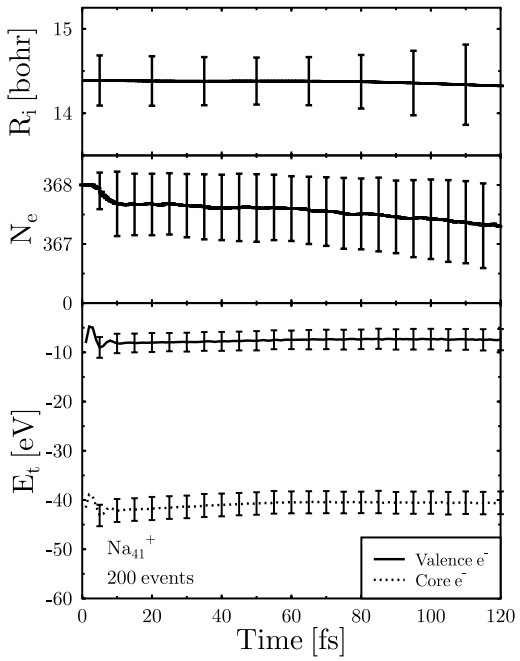

Fig. 1. Time evolution of ground state properties of a Na_{41}^+ cluster sampled from 200 events. Sigmas are $\sigma_v = 6.5$ bohr, $\sigma_c = 1$ bohr, $\sigma_i = 1$ bohr. Top: radius; middle: number of electrons inside cluster; bottom: mean potential energies with standard deviation for valence and core electrons.

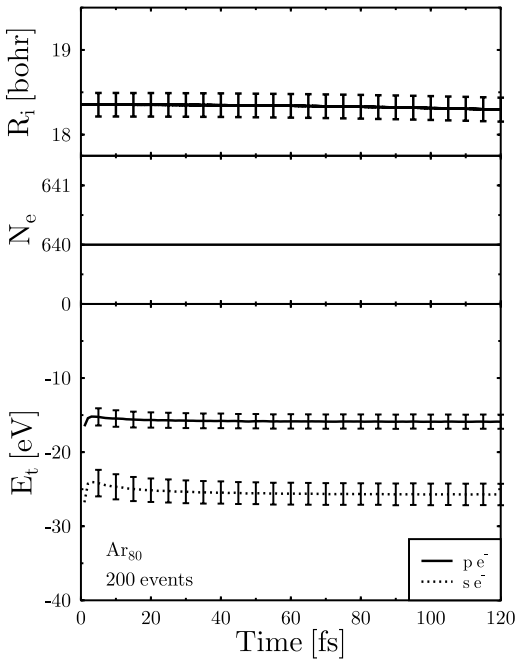

Fig. 2. Same as Figure 1 for an Ar_{80} cluster with $\sigma_p = 1.5$ bohr, $\sigma_s = 0.9$ bohr, $\sigma_i = 1.4$ bohr. Potential energies now refer to electrons of p and s levels.

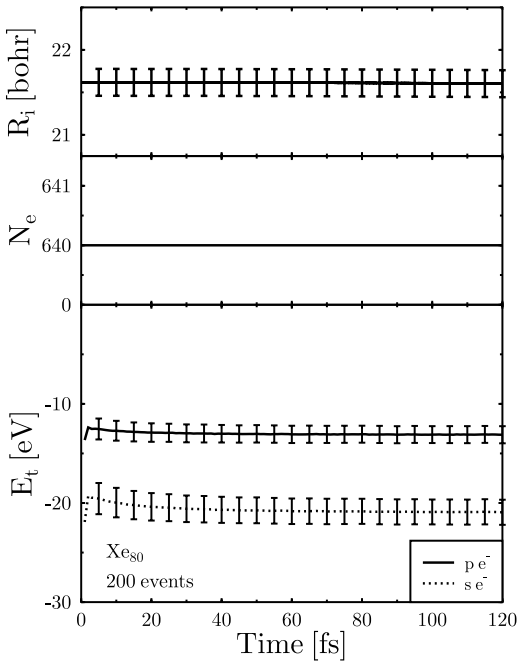

Fig. 3. Same as Figure 2 for a Xe_{80} cluster and $\sigma_p = 1.8$ bohr, $\sigma_s = 1.1$ bohr, $\sigma_i = 1.7$ bohr.

$\sigma_p/a_0 = 1.74$ for Ar, and $\sigma_s/a_0 = 0.94, \sigma_p/a_0 = 2.1$ for Xe.

As the second and final step comes the fine-tuning with respect to a cluster. To prepare the initial state of the cluster these values are now taken as starting point. After the stochastic sampling of the ion in a sphere of radius R all electrons belonging to an atom are distributed on the surface of a sphere of radius r about the ion avoiding again close distances between these electrons during the sampling process. The radius r is either r_c, r_s or r_v, r_p. It is deduced as an effective hydrogen-like orbit of an electron in the field of all other particles of the same atom and a shell energy ϵ, i.e. $r_v/a_0 = -13.6\ \mathrm{eV}/\epsilon_v$ etc. The corresponding values are also given in Table 1. The valence electrons in the Na-cluster are initialized as delocalized electrons by stochastically distributing them — in the same manner as the ions — over the whole cluster sphere. To obtain a good stability of the clusters the widths $\sigma_{v,p}, \sigma_{c,s}$ are fine tuned by monitoring the temporal evolution in MD runs for the whole cluster and with all Coulomb interactions, but in absence of any external perturbation ($\mathbf{E}_{\mathrm{laser}} = 0$). The adjusted and finally used $\sigma_{v,p}$ and $\sigma_{c,s}$ can be found in Table 1.

3.1 Stability

Examples for the achieved stability of the clusters are presented in Figures 1–3. Here the averaged total single particle energies E_t, the number of electrons in the cluster N_e and the ionic cluster radius R_i with

$$R_i^2 = \frac{5}{3}\left[\frac{1}{N_i}\sum_I r_I^2 - \left(\frac{1}{N_i}\sum_I r_I\right)^2\right] \qquad (5)$$

have been recorded from such MD runs over a time span of 120 fs. The above mentioned stochastic sampling leads

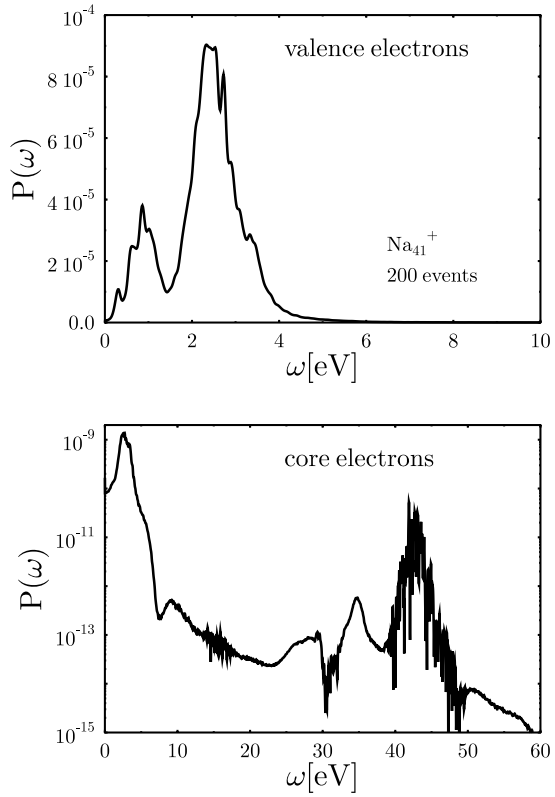

Fig. 4. Fourier transforms of center of mass for an initial kick of $\delta p_z = 1.5$ eV; top: valence electrons; bottom: core electrons.

to surprisingly stable systems. We typically observe only small variations of the system radius of less than 1% and no (Ar, Xe) or negligibly small (a fraction of a percent for Na) electron emission. The single particle energies E_t show fluctuations of a few eV (see the error-bars) but almost stationary mean values. As the electrons have not been initialized directly on top of the ions and due to the interaction between the particles of different atoms the E_t differ somewhat from their design values ϵ_v and ϵ_c.

3.2 Linear response

As a test of the dynamic ground state properties, we have evaluated the optical response by recording the dipole moments after an instantaneous initial excitation by a slight displacement of the electron cloud with respect to the ionic background [21]. Both the dipole moment of the valence electrons and the core electrons have been recorded and analyzed separately. One observes the expected oscillating behavior typical of optical response. The related dipole spectra are shown in Figure 4 for the Na_{41}^+ cluster. The dipole spectrum of the valence electrons shows quite appropriately the all dominating Mie surface plasmon resonance. Its frequency lies around 2.5 eV which compares very well with the experimental value of 2.65 eV [22] and with the 2.75 eV from calculations [23]. This plasmon frequency can be seen again in the spectrum of the core electrons (lower panel of Fig. 4) which are weakly coupled to the collective motion of the valence electrons (mind the strongly reduced amplitude of the core signal as compared to the valence one). The second peak in the core signal, which appears at a much higher frequency of about 42 eV, is associated with the oscillations of the core electrons in the minimum of the ionic potential at $|\mathbf{r}_I - \mathbf{r}_c| = 0$. The stability of the cluster and the acceptable optical response are already quite satisfying and obviously suffice for the high excitation domain we aim at studying.

4 Dynamics at laser irradiation

4.1 Electron emission at low intensities

The next step is to consider dynamics in an intermediate domain, namely above the linear response domain but still below the high laser intensities at which the systems are violently blown away. This intermediate energy domain was already explored in various aspects by means of microscopic calculations both at a quantal [26] and a semi classical (VUU) level [25]. It was shown, in particular, that at sufficiently high laser intensities, electron emission was dependent on the level of treatment of electron dynamics. The account of dynamical electron correlations within VUU was thus shown to notably enhance electron emission at laser frequencies matching the plasmon frequency, as compared to a pure mean field approach [25]. We have thus redone the calculations of [25] with our MD model in order to see how it compares with these former calculations. Results are presented in Figure 5. The agreement is remarkable, even from a quantitative point of view. Indeed we clearly observe resonant emission around the plasmon frequency. As noted above the MD plasmon frequency is a bit red shifted as compared to the microscopic one. But once accounted for the shift (of order 0.4 eV) the behavior and amplitude of resonant emission around the plasmon become fully comparable. It should in particular be noted that the maximum numbers of emitted electrons at plasmon peak are very close in MD and VUU calculations. This point is worth being emphasized. Indeed both calculations (MD and VUU) rely on basically different approaches. The VUU calculation treats electron correlations approximately in terms of a Boltzmann-like collision integral. By definition the MD approach includes all correlations but at a fully classical level. The interesting point here is that the agreement between the two approaches validates mutually both, because both involve rather different approximations. It is also interesting to check which kind of electrons are involved in the emission, remembering that in the VUU calculations only valence electrons are involved. In the MD calculation the situation is similar: only the valence electrons are emitted in the presented case. The situation of course evolves with the laser intensity. As we shall see below, for sufficiently high laser intensity we also observe core electron emission.

The spectral selectivity of the electron emission yield depends sensitively on the laser intensity [27]. Narrow lines are well resolved for low intensities. The width of the emission pattern grows larger with increasing intensity until

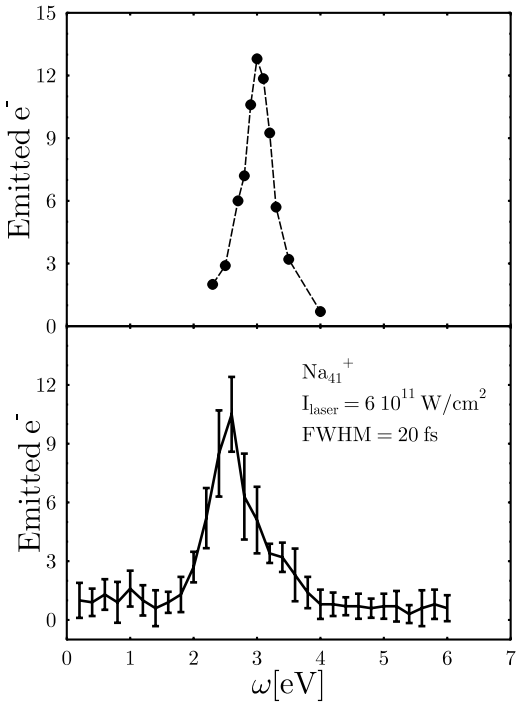

Fig. 5. Comparison of the number of emitted electrons as a function of frequency for VUU (top, Gaussian pulse, $FWHM = 20$ fs, $I = 6 \times 10^{11}$ W cm^{-2}, Mie frequency is given for 2.88 eV. Points are from Giglio et al. [24,25]) and MD (bottom, see figure for laser parameters, Mie frequency is given for 2.5 eV) cases.

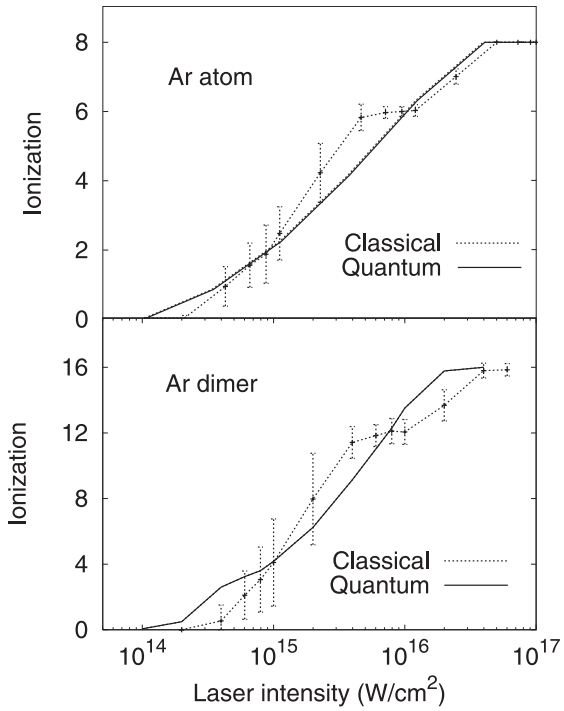

Fig. 6. Ionization of an Ar atom (upper) and Ar_2 dimer (lower) by a laser pulse with frequency of 3 eV and pulse length $FWHM = 50$ fs drawn versus intensity (in units of W/cm^2). Compared are fully quantum mechanical TDLDA calculations (using eight active electrons for each Ar atom) with the classical MD simulations. The results from MD stem from an ensemble calculation. The variation within the ensemble is indicated by error bars (covering minimum and maximum value).

any structure is dissolved after one has crossed the critical point from the frequency dominated regime to the field dominated regime [28]. We have checked these trends and find that the MD simulations behave in that respect precisely as the full TDLDA and the VUU simulations.

4.2 High intensity laser irradiation

4.2.1 Atomic and molecular examples

As a starting point for discussing the high intensity laser domain we continue to analyze the validity of our MD approach by considering electron emission from simple systems, namely monomer and dimers. Such simple cases can also be treated at a quantal TDLDA level which allows a direct comparison. This is achieved on two examples in Figure 6 for the particular case of argon where we present the total electron emission as a function of laser intensity.

At first glance, we see that MD ionizations are comparable to the quantal ones, both qualitatively and, to a large extent, quantitatively. It is noteworthy, in particular, that the intensity range on which ionization takes place is quite similar in both approaches. At second glance, one can nevertheless see that the two calculations differ in some details. First, the slope of ionization as a function of intensity is larger in the classical case than in the quantal one. Second, one observes a step in the classical calculations which reflects the sequential depopulation of the occupied states. The quantal calculation, on the other hand, shows a much smoother behavior, both in terms of intensity range and energy levels. This is clearly a quantum effect which softens the transition, e.g., by tunneling ionization somewhat before the classical barrier is reached. All in all the remarkable agreement between the quantal and classical approaches again validates our MD model, both in the low and high laser intensity regime. We can now safely turn towards the case of clusters in intense laser fields.

4.2.2 Cluster ionization

As a first step of analysis we compute the total ionization of given clusters as a function of laser intensity. Results are shown in Figures 7 to 9 for sodium, argon and xenon. All cases behave rather similarly, although we observe some differences, in particular between the metallic and the rare gas cases. For the sodium cluster, electron emission shows a steady slope from low intensities on. That is due to the ionization of the easily accessible valence electrons. The yield increases steeply as soon as the field strength suffices to break up the core which happens around an intensity of 10^{16} W cm^{-2}. The kink happens to occur at the point where about 40 electrons are removed which agrees with the number of initially given valence electrons.

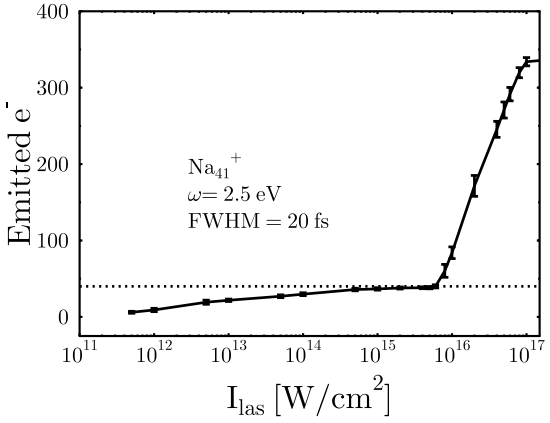

Fig. 7. Number of emitted electrons as a function of intensity for Na_{41}^+ clusters (data averaged over 3 events/point, pulse shape is $\cos^4$).

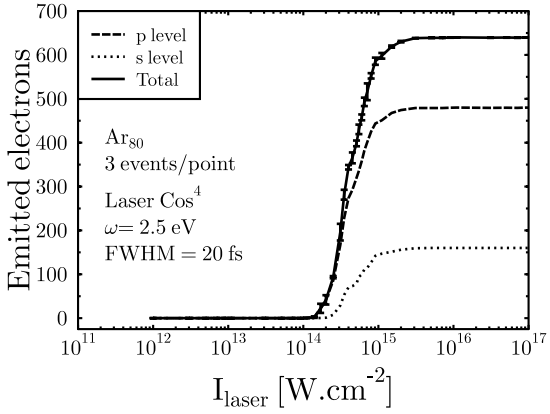

Fig. 8. Same as Figure 7 for Ar_{80} clusters.

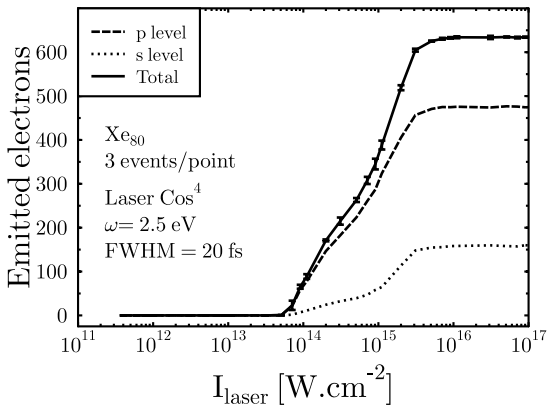

Fig. 9. Same as Figure 7 for Xe_{80} clusters.

The strong increase in emission is necessarily due to core electrons. The situation is slightly different in the case of rare gases which show a similarly steep increase but a totally flat trend for lower intensities. There are no softly bound valence electrons around which could easily contribute to ionization. The threshold intensities are around 10^{14} W cm^{-2} and a bit higher for Ar than for Xe as to be expected from the ionization potentials. Somehow surprising and on a first glance contradictory is the much steeper increase of the electron emission in Ar. We attribute this to a more efficient ionization by stronger electron-electron collisions in the Ar cluster due to its higher density and the lower $\sigma_{s,p}$ of the electrons. But here further investigations are needed for definite answers. At intensities above 5×10^{15} W cm^{-2} all active electrons which have been taken into account in our present studies (640 in total for both rare gas clusters) are emitted. In the case of sodium this point is not yet reached below 10^{17} W cm^{-2}.

There exist already some experimental [29] and theoretical [30,31] investigations on ionization of Xe clusters by intense laser pulses. We have compared results from our model with those and we report the findings in due brevity: we find less ionization as in the MD simulations of [30]. However, comparing with [31] for one well defined laser pulse, we find somewhat more ionization. Unfortunately, the major difference lies at the side of neutral species which is not accessible experimentally. The comparison done by [31] to the data of [29] implies an involved averaging procedure over laser pulse characteristics which makes a direct comparison difficult. A simpler comparison to experiments is nevertheless possible by considering the lower intensity results on electron emission from irradiated sodium clusters as studied in [32]. These experiments focused on Na_{93}^+ at laser intensities of order 10^{10} W cm^{-2}. Net electron emission remains rather limited in these cases (typically 1 to 4 electrons) and its analysis is thus quite demanding. Quantum TDLDA calculations [33] failed to reproduce these data properly, most probably because of the role played by electron–electron collisions and possibly because of the relation of the laser frequency to the dipole plasmon. Once this relation is properly accounted for, our MD calculations show a remarkable agreement with experimental data, as will be detailed in a forthcoming publication. As a conclusion, these various comparisons indicate that there is still a lot of work to be performed to align the various approaches. Direct comparisons to experiments show that the results of [31] as well as ours perfectly match experimental data, but in different systems, while they do not match with each other when compared directly. This puzzle has yet to be solved. Direct microscopic inputs (as obtained from quantum TDLDA or VUU calculations) are to be taken as complementing benchmarks. Such theories are unfortunatly only marginally accessible for rare gases, but the comparisons we have performed between these microscopic theories and our MD (for small systems yet) show that our MD calculations (in Na and Ar) perform as they should. We are thus confident that our MD model (which benefits from a great simplicity and transparency) is able to bring some important piece of information in the open question of the understanding of the dynamics of clusters in intense laser fields.

4.2.3 Coulomb explosion

Let us now examine in more detail the mechanisms of explosion of the irradiated clusters. In this high intensity

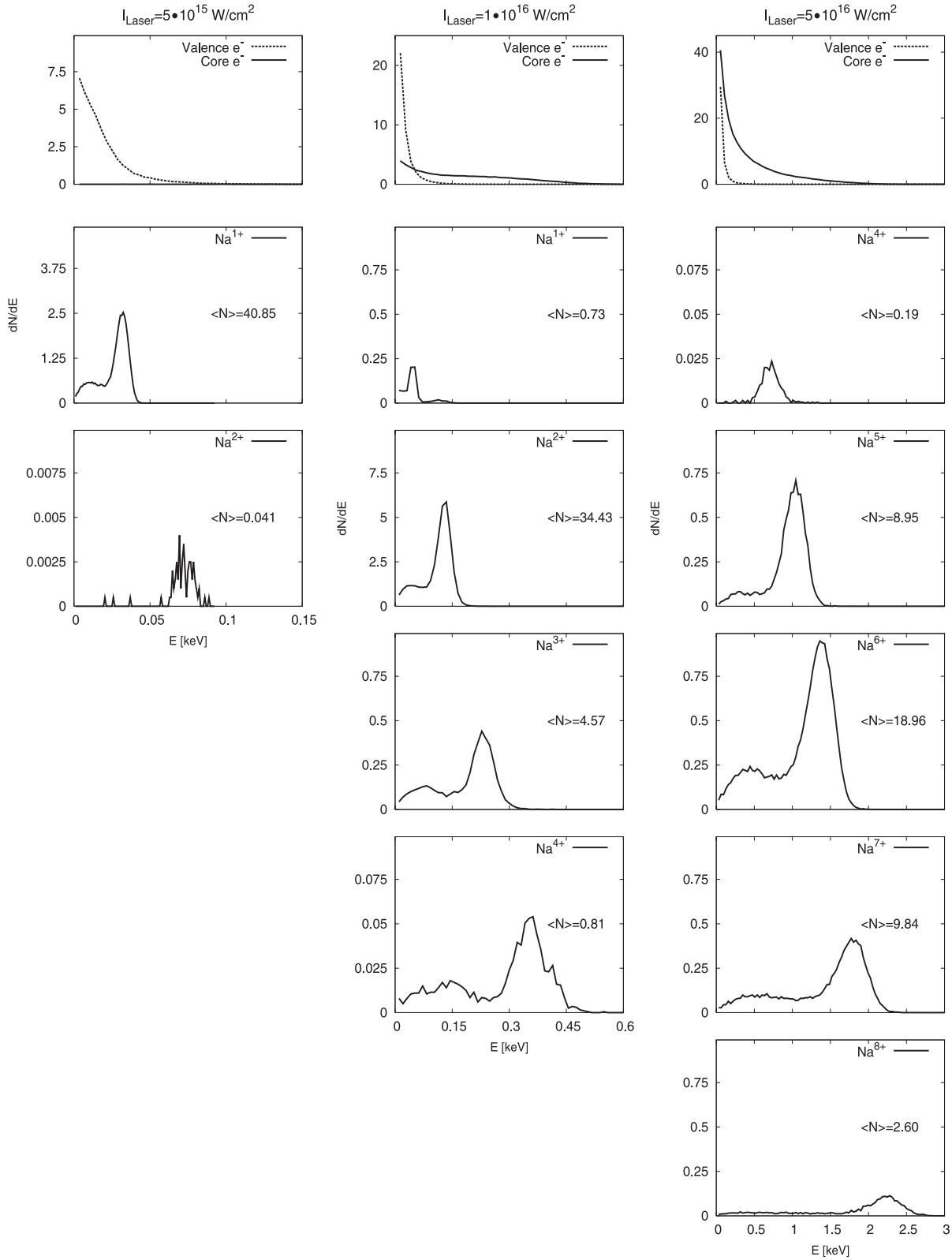

Fig. 10. Comparison of energy spectra of electrons (top panel) and selected ions (lower panels) for Na_{41}^{+} clusters obtained from 2000 events in each case of laser intensities $I = 5 \times 10^{15}$ W cm^{-2} (left column), $I = 1 \times 10^{16}$ W cm^{-2} (middle column) and $I = 5 \times 10^{16}$ W cm^{-2} (right column). The photon energy was $\omega = 2.5$ eV and the pulse width 20 fs (FWHM, $\cos^4$). Top panel: valence electrons is dashed line, Core electrons is solid line. Lower panels: dN/dE (effectively $N(E)$) for the different emerging ionic charge states. $N(E)$ is normalized so that $(\Sigma N(E))/N = 1$, $\langle N \rangle$ denotes the average number of ions in the specified charge state.

domain the expected scenario is a disintegration of the irradiated cluster by Coulomb explosion. This is found indeed in all our MD simulations. The experimentally observable signal of Coulomb explosion can be found in the energies of the emitted fragments. We thus have studied in detail the fragment kinetic energies, for laser intensities leading to cluster disintegration. The test case is Na_{41}^{+} at three laser intensities between 5×10^{15} W cm^{-2} and $I = 5 \times 10^{16}$ W cm^{-2}. Figure 10 shows typical results. The uppermost panel shows the kinetic energy spectra of electrons and the panels below the kinetic energy spectra of the ions at their various charge states. Each column of the figure corresponds to one given laser intensity. The maximum charge state attained of course depends on the laser intensity. In the present cases we have recorded spectra with significant statistics for charge states up to 2^+ at the lowest intensity and up to 8^+ at the highest intensity (the largest possible charge state in our model, 9^+, did not appear in amounts above statistical significance).

Electron spectra exhibit somewhat different shapes involving dominantly low energy electrons. This is especially true the higher the laser intensity. For sake of completeness, we have furthermore separated valence from core electron contributions. The valence electrons exhibit significantly lower energies than core electrons. This is due to the different initial binding and the related different widths. The smaller width of the core electrons results in stronger electron-ion collisions and yields an enhanced energy deposit due to a larger inverse Bremsstrahlung absorption of laser energy [34].

The case of ions is somewhat different. All ionic spectra look qualitatively similar with a relatively well marked peak and a low energy tail extending up to almost zero energy. The most striking result is here the linear dependence of the (average) ionic kinetic energy for a given ionic charge state with the ionic charge state, see e.g. the middle and right columns in Figure 10. We also find that the total kinetic energy of the ions turn out to depend quadratically on the average ionic charge which, once more, is a signature of a Coulomb explosion. Both features together are clear signatures of a Coulomb explosion starting for all intensities at about the same configuration. A quick estimate of the total kinetic energies shows that the starting point is near the ground state cluster radius. This complies with the fact that the majority of emitted electrons has left the cluster short after the end of the laser pulse, at a time where ionic motion has not yet evolved much.

5 Conclusions

We have presented a simple classical molecular dynamics (MD) model for the description of clusters in strong laser fields. The model describes all interacting particles by means of Gaussian density distributions of various widths, depending on the nature of the particle (ion, valence, core electrons) and interacting via the bare Coulomb interaction. This approach is used to consider both rare gas and metal clusters. We have shown that this simple model provides a surprisingly good description of cluster properties, including the low energy domain (ground state stability, optical response). The model performs even better in the true dynamical situations and at high excitation where it is designed for. At intermediate laser intensities it reproduces earlier microscopic results obtained in a semi classical approximation including dynamical correlations. At higher laser intensities, we have checked it against quantum mechanical results concerning ionization of very simple systems like atom and dimer of rare gases and found a satisfying agreement. This set of test cases and comparisons altogether shows that this molecular dynamics is reliable and can be used to study the response of clusters in strong electromagnetic fields. We have given some examples of applications in the cases of Ar, Xe and Na. We have especially discussed the results in Na where we performed systematics as a function of laser intensities. In all considered cases we have found a scenario of cluster disintegration in terms of Coulomb explosion.

This work was supported by the French-German exchange program PROCOPE, number D/0333667, the Institut Universitaire de France and the CNRS program "Matériaux" (CPR-ISMIR). One of the authors (ES) also thanks the Alexander von Humboldt foundation for support. Another author (PGR) acknowledges support from a Gay-Lussac/Humboldt prize.

References

1. P.-G. Reinhard, E. Suraud, *Introduction to Cluster Dynamics* (Wiley, New York, 2003)
2. M. Lezius, S. Dobosz, D. Normand, M. Schmidt, Phys. Rev. Lett. **80**, 261 (1998)
3. T. Ditmire, J.W.G. Tisch, E. Springate, M.B. Mason, N. Hay, R.A. Smith, J. Marangos, M.H.R Hutchinson, Nature **386**, 54 (1997)
4. L. Köller, M. Schumacher, J. Köhn, S. Teuber, J. Tiggesbäumker, K.-H. Meiwes-Broer, Phys. Rev. Lett. **82**, 3783 (1999)
5. A. McPherson, T.S. Luk, B.D. Thompson, A.B. Borisov, O.B. Shiryaev, X. Chen, K. Boyer, C.K. Rhodes, Phys. Rev. Lett. **72**, 1810 (1994)
6. S. Dobosz, M. Lezius, M. Schmidt, P. Meynadier, M. Perdrix, D. Normand, J.-P. Rozet, D. Vernhet, Phys. Rev. A **56**, R2526 (1997)
7. J. Zweiback et al., Phys. Rev. Lett. **85**, 3640 (2000)
8. S.A. Buzza, E.M. Snyder, D.A. Card, D.E. Folmer, A.W. Castleman Jr, J. Chem. Phys. **105**, 7425 (1996)
9. D.A. Card, E.S. Wisniewski, D.E. Folmer, A.W. Castleman Jr, J. Chem. Phys. **116**, 3554 (2002)
10. M. Belkacem, M.A. Bouchenne, P.-G. Reinhard, E. Suraud, Encycl. Nanosc. Nanotechn. **8**, 575 (2004)
11. T. Ditmire, T. Donnelly, A.M. Rubenchik, R.W. Falcone, M.D. Perry, Phys. Rev. A **53**, 3379 (1996)
12. M.A. Lebeault, J. Viallon, J. Chevaleyre, C. Ellert, D. Normand, M. Schmidt, O. Sublemontier, C. Guet, B. Huber, Eur. Phys. J. D **20**, 233 (2002)
13. F. Megi, M. Belkacem, M.A. Bouchene, E. Suraud, G. Zwicknagel, J. Phys. B **36**, 273 (2003)
14. M. Rusek, H. Lagadec, T. Blenski, Phys. Rev. A **63**, 013203 (2000)

15. K. Ishikawa, T. Blenski, Phys. Rev. A **62**, 063204 (2000)
16. L. Poth, A.W. Castleman Jr, J. Phys. Chem. A **102**, 4075 (1998)
17. I. Last, J. Jortner, Phys. Rev. A **62**, 013201 (2000)
18. U. Saalmann, M. Rost, Phys. Rev. Lett. **89**, 133401 (2002)
19. L. Verlet, Phys. Rev. **159**, 98 (1967)
20. `http://xray.uu.se/hypertext/EBindEnergies.html`, `http://physics.nist.gov/PhysRefData/IonEnergy/tblNew.html`
21. F. Calvayrac, P.-G. Reinhard, E. Suraud, Ann. Phys. (NY) **255**, 125 (1997)
22. H. Haberland, M. Schmidt, Eur. Phys. J. D **6**, 109 (1999)
23. E. Giglio, P.-G. Reinhard, E. Suraud, Ann. Phys. (Leipzig) **11**, 291 (2002)
24. E. Giglio, P.-G. Reinhard, E. Suraud, J. Phys. B **34**, 1253 (2001)
25. E. Giglio, P.-G. Reinhard, E. Suraud, Phys. Rev. A **67**, 43202 (2003)
26. F. Calvayrac, P.-G. Reinhard, E. Suraud, C.A. Ullrich, Phys. Rep. **337**, 493 (2000)
27. C.A. Ullrich, P.-G. Reinhard, E. Suraud, J. Phys. B **30**, 5043 (1997)
28. P.-G. Reinhard, F. Calvayrac, C. Kohl, S. Kümmel, E. Suraud, C.A. Ullrich, M. Brack, Eur. Phys. J. D **9**, 111 (1999)
29. H. Wabnitz et al., Nature **420**, 482 (2002)
30. D. Bauer, J. Phys. B **73**, 3085 (2004)
31. Ch. Siedschlag, J.M. Rost, Phys. Rev. Lett. **93**, 043402 (2004)
32. R. Schlipper, R. Kusche, B. von Issendorff, H. Haberland, Appl. Phys. A **72**, 255 (2001)
33. A. Pohl, P.-G. Reinhard, E. Suraud, J. Phys. B **37**, 3301 (2004)
34. V.P. Krainov, M.B. Smirnov, Phys. Rep. **370**, 237 (2002)